

To be appeared as Publ. Astron. Soc. Japan 52, L25-L30 (2000)

Unusual Properties of X-Ray Emission near the Galactic Center

Yasuo TANAKA

*The Institute of Space & Astronautical Science, 3-1-1 Yoshinodai, Sagamihara, Kanagawa
229-8510,*

*Max-Planck Institut für Extraterrestrische Physik, D-85748 Garching, Germany
E-mail(Y.T.): ytanaka@mpe.mpg.de*

Katsuji KOYAMA

Dept. of Physics, Kyoto University, Sakyo-ku, Kyoto 606-01

Yoshitomo MAEDA

*Dept. of Astronomy & Astrophysics, Penn State University, University Park, PA
16802-6305, U.S.A.*

and

Takashi SONOBE

Fujitsu Ltd., 4-1-1 Kamikodanaka, Nakahara-ku, Kawasaki, Kanagawa 211-8588

ABSTRACT

The X-ray spectrum in a $1^\circ \times 1^\circ$ region of the Galactic center observed with the ASCA satellite is examined in detail, following the first report by Koyama et al. (1996, AAA 65.155.208). The observed spectrum contains prominent emission lines from helium-like and hydrogen-like ions of various elements, and is essentially the same all over the region. If the observed spectrum is thermal emission from hot plasmas, it requires multi-temperature plasma components, each at a different degree of ionization and with a different amount of absorption. The absence of adiabatic cooling and of systematic changes in the degree of ionization over the region is against the Galactic center origin of hot plasmas. A significant broadening of the helium-like and hydrogen-like iron K-lines is confirmed. The line width corresponds to a rms velocity of $\sim 3300 \text{ km s}^{-1}$, which far exceeds the sound velocity in a plasma of $kT \sim 14 \text{ keV}$ measured with the Ginga satellite. These facts cast doubt on a thermal origin of the observed X-ray emission.

Subject headings: Galaxy: center — line: profiles — X-ray: galaxies

1. Introduction

The Galactic center (GC) region is unique in various aspects (for reviews see Genzel et al. 1994; Mezger et al. 1996). Eckart and Genzel (1996) discovered the presence of a massive black hole of $\sim 2.5 \times 10^6 M_{\odot}$ coincident with the compact radio source Sgr A*. Although the central black hole is currently inactive, the complex features in the GC region may reflect its past activities.

The first detailed X-ray imaging and spectroscopic observations of the GC region were carried out with the ASCA satellite. The first results were published by Koyama et al. (1996) (hereafter referred to as Paper I). As shown in Paper I, the X-ray brightness structures are strikingly similar to the radio brightness structures (see figure 1b of Paper I), strongly suggesting that the X-ray emission and the radio emission are physically connected in one way or another.

The ASCA observation also provided an X-ray spectrum of the GC region with unprecedented resolution (figure 2 in Paper I). The general properties of the X-ray spectrum were discussed in Paper I, based on models of thermal emission from hot plasmas. It was also mentioned in Paper I that the helium-like and hydrogen-like iron K-lines apparently show Doppler broadening. Since this is crucial for understanding the origin of the observed X-ray emission, a confirmation and further study of this line broadening is very important. In this paper, we re-examine the spectral data from the ASCA observation of the GC region, and discuss the results and implications.

2. Observed Spectrum

ASCA carries two types of imaging spectrometers, GIS and SIS (see Tanaka et al. 1995). In this work, we deal only with the SIS data for the higher spectral resolution. The SIS consists of two detectors, S0 and S1, respectively placed at the foci of two co-aligned X-ray telescopes. Both comprise four CCD chips (C0–C3) and cover a common square field of view of $\sim 22' \times 22'$. The ASCA observation of the GC region covered approximately $1^{\circ} \times 1^{\circ}$ ($\sim 150 \times 150 \text{ pc}^2$) of the GC in a mosaic of eight SIS fields with the pointing positions listed in table 1 (see figure 1a of Paper I). At the time of this observation (1993 September 30–October 5), the measured FWHM was approximately 140 eV for the iron K α -line at 6.4 keV (or $\sigma \approx 60 \text{ eV}$). Data were screened according to the normal selection criteria. In addition, we required the cut-off rigidity to be greater than 8 GV. The exposure time for useful data of each field was between 14 ks and 20 ks, depending on the pointing position.

We constructed spectrum for each of the eight fields, after removing the detected point

sources. The background data were obtained from the work by Gendreau et al. (1995) based on observations of high galactic latitude regions. The background consists of the cosmic X-ray background (CXRB) and the instrument background. The latter contains fluorescence lines of iron and nickel, of which the nickel line is the strongest. The background was determined by adjusting the instrument background level so that the nickel line (7.48 keV) intensity would be equal to that in the observed spectrum. To do this, we summed all eight spectra together to allow an accurate measurement of the nickel line intensity. We have not applied galactic absorption to the CXRB spectrum. Though the low-energy absorption toward the GC region is quite significant, the effect is small above 2 keV owing to a good S/N ratio, except for the range above 7 keV. Thus, the derived spectrum for the entire GC region is shown in figure 1 (the same as figure 2 in Paper I).

The observed emission lines are identified with $K\alpha$ -lines of helium-like and hydrogen-like ions of silicon, sulphur, argon, calcium, and iron. The helium-like $K\beta$ -lines of silicon, sulphur, and argon are also significantly visible, as marked respectively in figure 1. In addition, a significant 6.4-keV fluorescent iron $K\alpha$ -line is present. The best-fit model comprising emission lines and a continuum is also shown in Fig. 1. The continuum is expressed by a power-law with a photon index of ~ 1.2 . If approximated by a thermal bremsstrahlung spectrum, the electron temperature is higher than 10 keV, but unbound because of the limited energy band. Previously, Yamauchi et al. (1990) obtained a temperature of 14 ± 1 keV for the same GC region from observations over a wider energy band up to 20 keV with the Ginga satellite. We use this temperature for thermal emission in later discussions.

For the purpose of supplementing Paper I, the spectrum for each individual field is presented in figure 2, in which the vertical scale is successively shifted. The background determined for the summed spectrum was subtracted from each observed spectrum. As noted in Paper I, these spectra are very similar to each other, except for the region of Srg B2, which shows a distinctly different spectrum, and is not included in figure 2. This region exhibits a signature of strong X-ray reflection with a very hard continuum and a pronounced 6.4 keV line (see Murakami et al. 2000). The model spectrum drawn on each spectrum is the best-fit

Table 1. The Galactic coordinates of the eight pointing positions

Position	l^{II}	b^{II}	Position	l^{II}	b^{II}
1	359.97	+0.01	5	359.83	-0.50
2	0.33	+0.22	6	359.73	-0.15
3	0.51	-0.08	7	359.47	+0.09
4	0.15	-0.28	8	359.81	+0.31

to the summed spectrum (shown in figure 1), except that the absorption, normalization and the 6.4-keV line intensity are individually determined. It is noticed that the fit is not good near the silicon line (~ 1.9 keV) for Position 3 and 7, where the absorption is particularly strong. The fit improves by considering a distributed absorber within the emission region instead of placing all of the absorber in front of the emission region. For a further test, the equivalent widths of the prominent lines (helium-like Si, S, Ar, Fe, and hydrogen-like Fe) were individually determined for each field. The measured equivalent widths for each element were found to be the same within $\pm 30\%$ over the entire region observed, except for a systematic trend that the iron line intensity slightly decreases with the Galactic latitude. Thus, one can conclude that the intrinsic spectrum is essentially identical over the entire $1^\circ \times 1^\circ$ area around the GC. This also justifies the summation of all individual spectra to obtain the best statistical accuracy (figure 1).

3. Iron Line

Table 2. Energies of the iron K-lines and the line widths

true (keV)	observed (keV)	line width σ (eV)
Step 1 ———		
6.40	6.42 (6.41–6.43)	30 (0–47)
6.70	6.72 (6.70–6.73)	93 (69–120)
6.97	7.00 (6.96–7.04)	88 (62–120)
Step 2 ———		
6.40	6.42 (6.41–6.43)	27 (0–44)
6.70	6.72 (6.71–6.73)	78 (70–85)
6.97	fixed at 1.04 \times above	= above
7.48 *	7.53 (7.51–7.56)	36 (0–69) *

Step 1: Results obtained from all CCD chips.

Step 2: Results from the data, excluding S0C2 and S1C0 and Sgr A and the Position 3 field, where the two line energies are linked (see text).

* The fluorescent K-line of nickel in the instrumental background. The line width error is large due to poor statistics.

The numbers in parentheses are the 90% confidence limits.

The iron emission line complex consists of at least three lines, a fluorescent $K\alpha$ -line from low-ionization iron atoms (below XVII stage), $K\alpha$ -lines from helium-like and hydrogen-like

ions. A model fitting is performed to the observed eight-field summed spectrum (before background subtraction to preserve the best statistics) in the range 5–9 keV. We also took into account that the helium-like $K\alpha$ -line is a triplet (6.64 keV, 6.67 keV, and 6.70 keV), which are not resolved with the SIS energy resolution. For possible offsets in the energy scale, we kept the observed energy of the 6.70-keV line as a free parameter, while the energy ratios of the other two lines to 6.70 keV were fixed. The intensity ratios of the three lines are also fixed, taken from the calculation for $kT = 10$ keV by Masai (1984). The hydrogen-like line at 6.97 keV is a singlet, and the line energy was also kept free for fitting. A satisfactory fit was obtained with $\chi^2 = 92$ for 106 d.o.f. The thus-determined line energies and the line widths (Gaussian σ) are given in table 2 “Step 1”. The measured line energies are in excellent agreement with the true values within a very small calibration uncertainty. Including the weak fluorescence $K\beta$ line (7.05 keV) did not change the result. If, as a reasonable assumption, we fixed the ratio of the energies of the hydrogen-like and helium-like lines at that of the true values (6.97 keV/6.70 keV), keeping the observed 6.7-keV line energy free, and requiring the same width for both lines, we obtained a line width of 92 eV with a 90% confidence range of 85–101 eV.

The 6.4-keV line is most probably the fluorescence line emitted from cool matter, and is hence an intrinsically narrow line. (Note that the contribution from the 6.4-keV line in the internal background is negligibly small.) The observed line width of 30 eV is considered to be due to systematic offsets of the energy scale among eight SIS chips, since the 6.4-keV iron line and the 7.5-keV nickel line in the internal background also show a ~ 30 eV width.

As a next step for scrutinizing any possible systematic effects, we examined the data from each of the eight chips individually with respect to the energy calibration and resolution. To perform the examination, we excluded the Sgr A region, which is exceptionally bright as well as heavily absorbed, and also Position 3, which includes the giant molecular cloud Sgr B2, for the previously explained reason. All of the spectra in other fields were added for each SIS chip. Then, each summed spectrum was fitted individually in the same way as described above. As a result, we have found that two chips, S0C2 and S1C0, exhibit a weaker (hence less-defined) 6.4-keV line and somewhat broader helium- and hydrogen-like lines than the other six chips. For the rest, the energy scale is confirmed to be accurate within ± 20 eV. The data from these two chips are excluded, and all other data are summed again.

The same model as before was used for fitting. The result of the fit ($\chi^2 = 110$ for 108 d.o.f) is shown in figure 3, and the best-fit line energies and widths are given in table 2 “Step 2”. While the line-energy values remain the same as before, the widths of the 6.4-keV line and the helium-like and hydrogen-like lines are slightly reduced to 27 eV and 78 eV, respectively. The difference between the two widths is statistically quite significant. We thus

conclude that the broadening of the helium-like and hydrogen-like lines is real. Considering the width of the 6.4-keV line to be systematic, we obtained a Gaussian width, σ , of 73 ± 14 eV (90% confidence error) for these lines.

We investigated whether or not this broadening could result from a spatial variation of the line energy. The line energies were determined for each individual field, i.e. for the spectra shown in figure 2, except for Position 3. As a result, the energies of the 6.7-keV line are all consistent with being constant with a rms dispersion of ~ 11 eV. Therefore, for a possible spatial energy variation, the scale size of the variation should be smaller than an SIS field of $20' \times 20'$.

4. Discussion

The observed properties of the X-ray emission near to the GC are unusual in several respects. The spectrum is very hard. If it is thermal emission, the temperature could be ~ 14 keV according to the previous Ginga observation (Yamauchi et al. 1990), which is far higher than that of young supernova remnants. The presence of strong lines from silicon, sulphur and argon at this temperature requires either non-equilibrium ionization (*nei*) or multi-temperature components, or both. Employing the *nei* plasma model developed by Masai (1984), we find that a single-temperature *nei* plasma cannot account for the observed spectrum.

In the observed spectrum, not only the helium-like and hydrogen-like $K\alpha$ -lines of silicon, sulphur, argon, and iron, but also the helium-like $K\beta$ -lines of silicon, sulphur, and argon are resolved. The line intensity ratio, $I(\text{H-}K\alpha)/I(\text{He-}K\alpha)$, of each element is a function of the electron temperature, T_e , and the degree of ionization determined by $n_e t$, where n_e is the electron density and t the age of the plasma. Here, He- and H- denote helium-like and hydrogen-like, respectively. However, the line-intensity ratio $I(\text{He-}K\beta)/I(\text{He-}K\alpha)$ is a sole function of T_e . Therefore, for silicon, sulphur, and argon, the measured line intensities, $I(\text{He-}K\alpha)$, $I(\text{H-}K\alpha)$ and $I(\text{He-}K\beta)$, constrain both T_e and $n_e t$.

We attempted to see this constraint qualitatively for the lines of silicon, sulphur and argon separately, using the *nei* plasma code by Masai (1984). For each element, the energy range was limited to cover only those lines from the element. We assumed that the lines of an element come from a single-temperature plasma. The results are listed in table 3. Although the errors are relatively large, because of coupling between the parameters, the results indicate that each element requires a different temperature than others, hence demonstrating the necessity of multi-temperature components.

In reality, the situation is more complicated, since various temperature components contribute to the lines of each element. We attempted to reproduce the observed spectrum with a multi-component *nei* plasma model, but failed to obtain a reasonable fit. Besides, a fundamental problem exists. In order to reproduce the observed hard continuum, each temperature component inevitably requires a different amount of absorption than others, which is artificial and quite unrealistic. This is a serious problem in a multi-temperature plasma interpretation.

We have confirmed that the helium-like and hydrogen-like iron K-lines are broadened with $\sigma \approx 73$ eV. This corresponds to a rms velocity dispersion of ~ 3300 km s⁻¹ of iron ions. Broadening of the lines of lighter elements is not conclusive, because of decreasing resolution at lower energies. As discussed in Paper I, it is quite unlikely that the observed velocity dispersion is due to the thermal motion of ions, since it corresponds to a temperature of ~ 3 MeV. It is most probably due to bulk motions.

As shown in the previous section, no spatial variation is found in the iron line energy within a scale of at least 20' (~ 50 pc), implying that bulk motions at various directions are taking place within this scale. This is against large-scale systematic motion, such as rotation around the GC or directed (e.g. radial) streaming. If we assume the motion to be nearly random, the actual velocity dispersion would be even larger, ~ 5000 km s⁻¹, since the line width represents the line-of-sight velocity component.

If the observed X-rays are thermal emission, the plasma pressure is $\sim 7 \times 10^{-9}$ erg cm⁻³ for a temperature of ~ 14 keV and a density of ~ 0.3 electron cm⁻³, as derived from the emission measure (see Paper I). If magnetic fields on the order of mGauss are present, these plasmas are contained by the magnetic fields and will propagate along the field lines. This picture is consistent with the observed similarity in the brightness structure between X-rays and radio, the latter being synchrotron radiation by magnetically-trapped high-energy electrons. On the other hand, if the hot plasma were produced at the GC, as considered in

Table 3. Plasma temperature, $n_e t$ and abundance for the individual elements

Element	kT_e (keV)	$\log n_e t$	Abundance (solar)
Si	1.5 ± 0.3	11.1 ± 0.2	0.33 ± 0.4
S	2.2 ± 0.1	11.1 ± 0.1	0.29 ± 0.4
Ar	6.2 ± 0.7	11.1 ± 0.3	0.23 ± 0.4
Fe	14 (fixed)	11.8 ± 0.1	0.42 ± 0.3

* The errors are the 90% confidence limits.

Paper I, the plasma would be adiabatically cooled as it expands. This cooling is expected to be quite significant, but it is not observed. The observed spectrum appears to be the same everywhere. A possibility was discussed in Paper I to maintain the electron temperature through energy transfer from ions that carry most of the energy in an *nei* plasma. However, the collisional ionization would proceed during propagation. If the plasma moves at the inferred speed to ~ 100 pc away, the quantity $n_e t$ would increase by at least $2 \times 10^{11} \text{ cm}^{-3} \text{ s}$. This would be sufficient to change the emission line structure significantly, but no difference is found between the near and far sides of the GC. These facts are against a GC origin of the hot plasmas. An even more fundamental problem is that the observed velocity, either $\sim 3300 \text{ km s}^{-1}$ or $\sim 5000 \text{ km s}^{-1}$, greatly exceeds the sound speed in a 14-keV plasma ($\sim 1400 \text{ km s}^{-1}$). This makes it very unlikely that the line broadening is due to plasma motions.

The above discussions present critical problems concerning the thermal plasma origin of the X-ray emission near to the GC. An alternative interpretation has been presented by Tanaka, Miyaji, and Hasinger (1999), in which X-ray line emission through charge-exchange interactions of low-energy cosmic-ray heavy ions was considered. When a low-energy cosmic-ray ion of charge q undergoes a charge-exchange interaction with interstellar matter (mostly hydrogen), it captures an electron and becomes an ion of charge $q-1$ in an excited state, which subsequently settles to the ground state by emitting characteristic X-rays. Because the charge exchange has a very large cross section at low energies (e.g. Phaneuf et al. 1987), it is an efficient process for producing X-ray emission lines. The authors point out the similarity between the observed X-ray line intensity ratios for various elements and the cosmic and cosmic-ray abundance ratios. Also, the observed line broadening is explained in terms of a sharp energy dependence of the charge-exchange interaction cross section. The cross section is very steep, $\propto E^{-4.5}$, when $Eq^{-1/2} \gg 25 \text{ keV/nucleon}$, where E is the ion energy per nucleon. However, it is essentially constant for $Eq^{-1/2} < 25 \text{ keV/nucleon}$. Therefore, as ions slow down by ionizing the ambient medium, they undergo charge-exchange interactions preferentially at energies of around $25q^{1/2} \text{ keV/nucleon}$. For helium-like and hydrogen-like iron ions, this energy corresponds to $\sim 5000 \text{ km s}^{-1}$, fully consistent with that observed.

A crucial test can be provided by a precise measurement of the widths of the lines from the lighter elements, since the line width is expected to be proportional to $q^{1/2}$ in this scenario. On the other hand, the line width should be the same for all the lines, if it is due to plasma motions. New-generation high-performance X-ray astronomy missions may provide an answer.

We have shown that a hot plasma of the GC origin is unlikely, yet it shows a temperature that is too high for a locally produced plasma by supernovae. Moreover, the unusual properties of the observed X-ray emission cast doubt on a thermal origin. Tanaka, Miyaji,

and Hasinger (1999) also pointed out that the X-ray emission along the Galactic ridge shows a very similar spectrum to that near to the GC, suggesting the same origin for the extended X-ray emission along the entire Galactic plane. Identifying the origin of this X-ray emission is very important. It is probable that other spiral galaxies also exhibit similar X-ray emission. Such observations with the recent high-sensitivity missions will also provide valuable clues to solve the question.

References

- Eckart A., Genzel R. 1996, *Nature* 383, 415
- Gendreau K. C., Mushotzky R., Fabian A. C., Holt S. S., Kii T., Serlemitsos P. J., Ogasaka Y., Tanaka Y. et al. 1995, *PASJ* 47, L5
- Genzel R., Hollenbach D., Townes C. H. 1994, *Reports of Progress in Physics* 57, 417
- Koyama K., Maeda Y., Sonobe T., Takeshima T., Tanaka Y., Yamauchi S. 1996, *PASJ* 48, 249 (Paper I)
- Masai K., 1984, *AP&SS* 98, 367
- Mezger P. G., Duschl W. J., Zylka R. 1996, *A&AR* 7, 289
- Murakami H., Koyama K., Sakano M., Tsujimoto M., Maeda Y. 2000, *ApJ* 534, 283
- Phaneuf R. A., Janev R. K., Hunter H. T. 1987, in *Nuclear Fusion* (International Atomic Energy Agency, Vienna) p13
- Tanaka Y., Inoue H., Holt S. S. 1994, *PASJ* 46, L37
- Tanaka Y., Miyaji T., Hasinger G. 1999, *Astron. Nachr.* 320, 181
- Yamauchi S., Kawada M., Koyama K., Kunieda H., Tawara Y., Hatsukade I. 1990, *ApJ* 365, 532

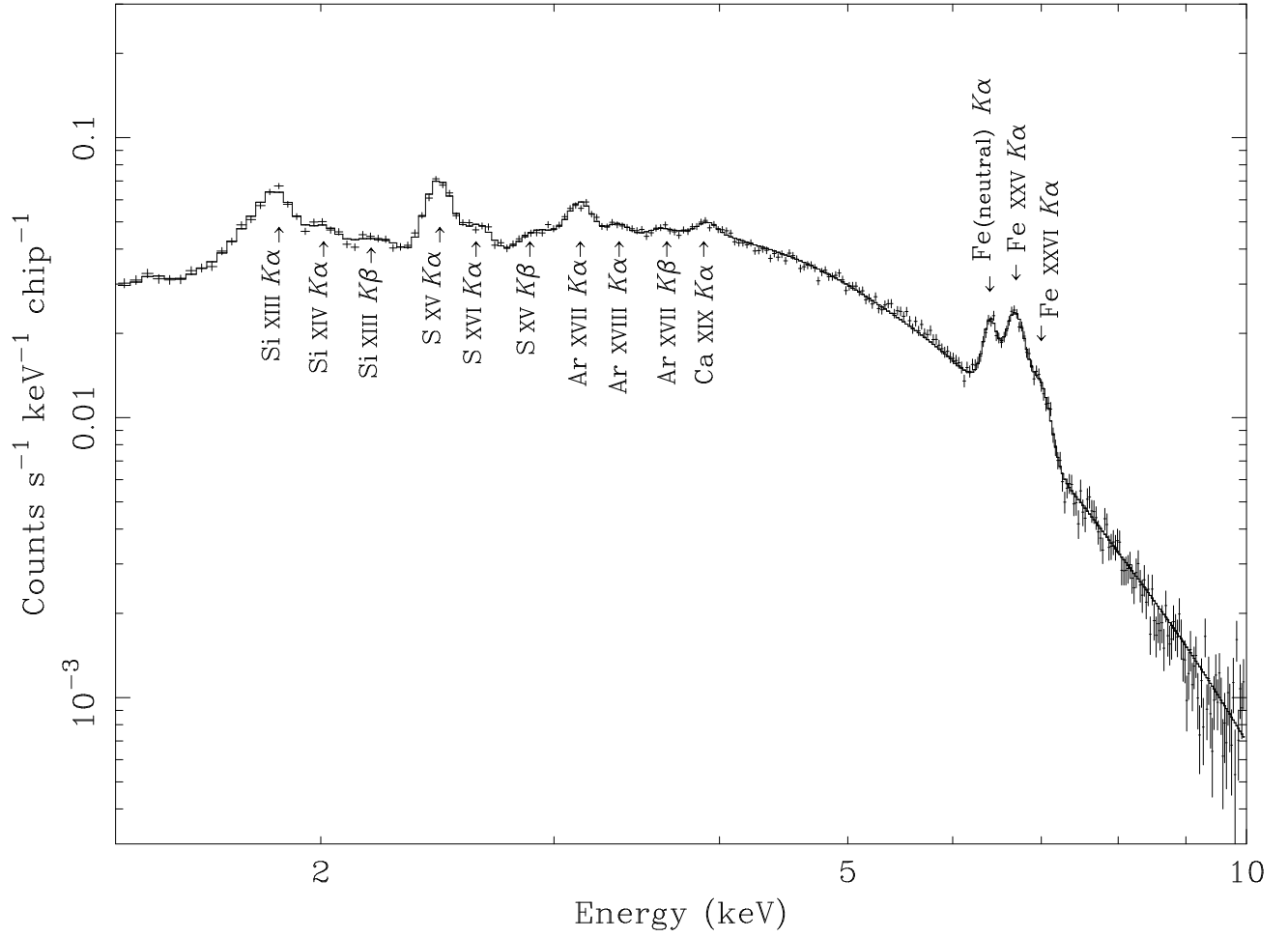


Fig. 1.— Spectrum for the entire GC region observed. The discrete source contributions have been removed. The identified emission lines are indicated, respectively. The best-fit model is also included.

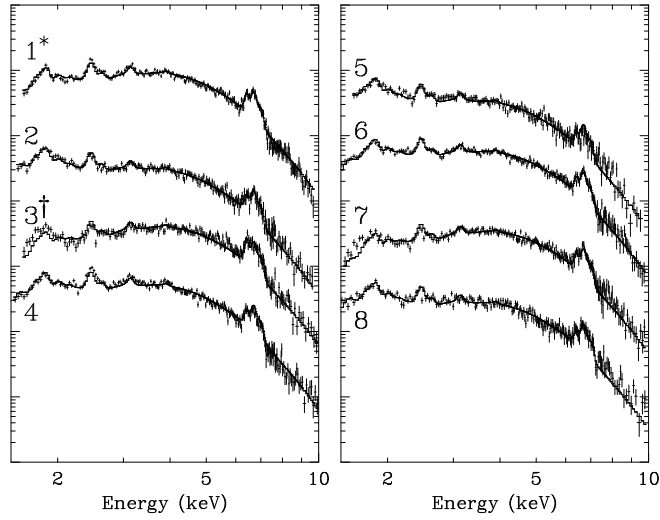


Fig. 2.— Observed spectra at eight pointing positions. The unit of the vertical axis is arbitrary.

(*): The spectrum for Position 1 excludes the Sgr A region.

(†): The spectrum for Position 3 excludes an area of Sgr B2.

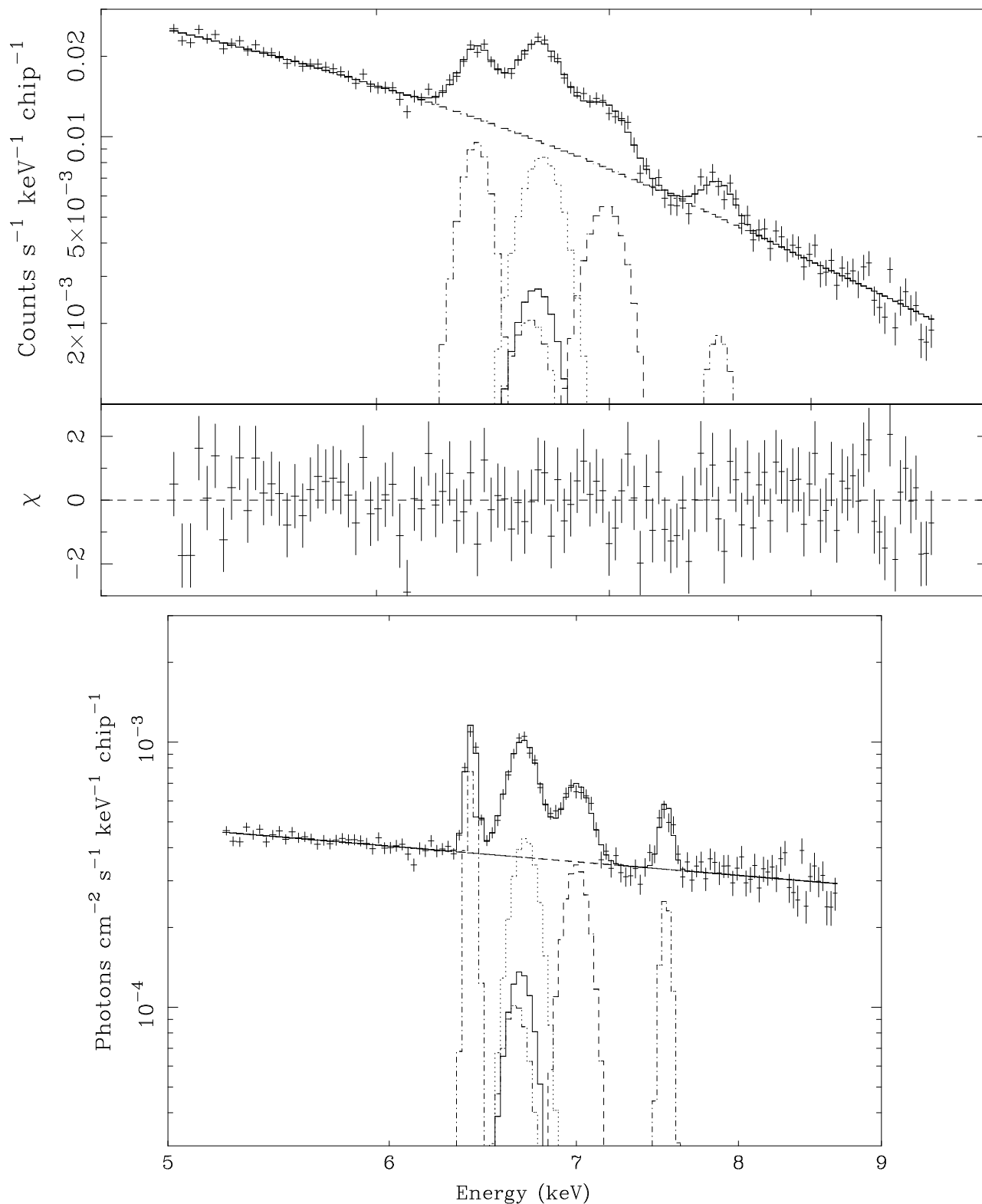


Fig. 3.— Upper panel: Best-fit to the observed iron line complex obtained with six qualified chips (see text), excluding the Sgr A region and the Position 3 field. The background is not subtracted, and the instrumental nickel line (7.48 keV) is also present. Lower panel: Same as the upper panel, but deconvolved with the energy response function of the SIS to